Sci. Technol. Adv. Mater. **11** (2010) 045005 (13pp) doi:10.1088/1468-6996/11/4/045005

A methodology to investigate the intrinsic effect of the pulsed electric current during the spark plasma sintering of electrically conductive powders

Antonio Mario Locci[1], **Alberto Cincotti**[1], **Sara Todde**[1], **Roberto Orrù**[1] **and Giacomo Cao**[1,2]

[1] Dipartimento di Ingegneria Chimica e Materiali, Unità di Ricerca del Consorzio Interuniversitario Nazionale di Scienza e Tecnologia dei Materiali (INSTM), and Unità di Ricerca del Dipartimento Energia e Trasporti del Consiglio Nazionale delle Ricerche (CNR), Università degli Studi di Cagliari, Piazza d'Armi, 09123 Cagliari, Italy
[2] CRS4—Centro di Ricerca, Sviluppo e Studi Superiori in Sardegna, Parco Scientifico e Tecnologico, POLARIS, Edificio 1, 09010 Pula (CA), Italy

E-mail: locci@dicm.unica.it and cao@visnu.dicm.unica.it

Received 27 April 2010
Accepted for publication 13 July 2010
Published 19 October 2010
Online at stacks.iop.org/STAM/11/045005

Abstract
A novel methodology is proposed for investigating the effect of the pulsed electric current during the spark plasma sintering (SPS) of electrically conductive powders without potential misinterpretation of experimental results. First, ensemble configurations (geometry, size and material of the powder sample, die, plunger and spacers) are identified where the electric current is forced to flow only through either the sample or the die, so that the sample is heated either through the Joule effect or by thermal conduction, respectively. These ensemble configurations are selected using a recently proposed mathematical model of an SPS apparatus, which, once suitably modified, makes it possible to carry out detailed electrical and thermal analysis. Next, SPS experiments are conducted using the ensemble configurations theoretically identified. Using aluminum powders as a case study, we find that the temporal profiles of sample shrinkage, which indicate densification behavior, as well as the final density of the sample are clearly different when the electric current flows only through the sample or through the die containing it, whereas the temperature cycle and mechanical load are the same in both cases.

Keywords: electric current, Joule effect, modeling, spark plasma sintering

Nomenclature

C_E	electrical contact conductance ($\Omega^{-1}\,m^{-2}$)
C_p	heat capacity ($J\,kg^{-1}\,K^{-1}$)
C_T	thermal contact conductance ($W\,m^{-2}\,K^{-1}$)
e	difference between set-point temperature and actual temperature (K)
F	mechanical load (N)
f	fraction of localized joule heat due to electrical contact resistance
H	height (m)
h	heat transfer coefficient ($W\,m^{-2}\,K^{-1}$)
I_{rms}	rms electric current (A)
J_{rms}	rms current density ($A\,m^{-2}$)
K_P	proportional gain of the PID controller ($A\,K^{-1}$)
k	thermal conductivity ($W\,m^{-1}\,K^{-1}$)

$\vec{n}$	surface area unit vector in the outward direction
P	applied mechanical pressure (N m^{-2})
q_c	heat flux due to the thermal contact resistance (W m^{-2} K^{-1})
q_e	localized joule heat flux due to the electrical contact resistance (W m^{-2} K^{-1})
R	radius (m)
r	radial coordinate (m)
S	surface area (m^2)
T	temperature (K)
T_0	initial ambient temperature (K)
t	time (s)
V_{rms}	rms voltage (V)
z	axial coordinate (m)

Greek letters

ΔT	temperature difference (K)
δ	sample shrinkage (m)
ε	relative density
Φ	cumulative fraction of total current flowing through a horizontal section with a radius r
φ	resistive rms voltage (V)
φ_0	resistive rms voltage between ends of the electrodes (V)
η	emissivity
ν	Stefan–Boltzmann constant (W m^{-2} K^{-4})
ρ	density (kg m^{-3})
ρ_{el}	electrical resistivity (Ω m)
τ_D	derivative time constant of PID controller (s)
τ_I	integral time constant of PID controller (s)

Subscripts

Al	aluminum
Al_2O_3	alumina
C	graphite
ss	stainless steel

1. Introduction

Spark plasma sintering (SPS) is a powder metallurgy process that is typically used for sintering a variety of materials including metals, ceramics, composites and polymers [1, 2]. In the SPS method, powders, which can be electrically conducting or insulating, are placed in a container (die, tube, etc) and heated by a pulsed electric current while applying uniaxial pressure. Conducting powders are heated by both the Joule effect and thermal conduction from the container, which is typically made of an electrically conducting material, whereas insulating powders are heated only through thermal conduction.

Regardless of the electrical conductivity of the powders to be sintered, it is often claimed that dense products with improved mechanical and physical properties are attainable in shorter times and at a lower temperature and pressure by SPS than by the conventional pressure-assisted sintering technique, i.e. hot pressing (HP). The main difference between SPS and HP is in the heating mode, as the powders (either electrically conducting or insulating) sintered by HP are heated exclusively through thermal conduction from the container. The container, in turn, is heated by thermal radiation from the heating elements of the furnace and/or the forced convection of hot gases.

However, while the feasibility of the SPS and its shorter sintering time have been clearly demonstrated, the other advantages relative to HP have usually been claimed without providing in most cases unequivocal experimental evidence. For instance, when comparing SPS and HP, the roles of temperature gradients and thermocouples positioning are often underestimated. As a result, the temperature experienced by the SPS and HP sintering compacts might be identical in several cases only nominally. In addition, the general advantages of SPS relative to HP have not been proved to be an intrinsic (i.e. non-thermal) effect of the applied pulsed electric current or a result of the higher heating rate achievable by SPS through the Joule effect. Consequently, the explanations given for the above-mentioned advantages of SPS relative to HP typically '*fall short of scientific adequacy*' [3].

On the other hand, some of the beneficial effects of the pulsed electric current applied in SPS apparatuses are typically accepted '*almost as a matter of faith*' [3]. In addition, the role of the electric current, which markedly distinguishes the SPS of electrically conducting and insulating powder, has been largely ignored. Therefore, it is not surprising that despite the large number of SPS publications (>1600) and interpretations of its mechanism (see, for example [3–5]), the effect of the electric current has not yet been unambiguously clarified.

Thus, a basic understanding of the SPS process is yet to be achieved and, in particular, the intrinsic role of the pulsed electric current applied in this process remains controversial. This is because under the typical experimental conditions of SPS temperature and electric current are not independent parameters so that the intrinsic role of the electric current cannot be separated from the thermal (Joule) effect.

To separate the thermal and non-Joule effects of the electric current during the SPS, the spacers/plungers/die/sample (ensemble) configuration should be carefully designed. The intrinsic effect of the electric current on sintering may then be evidenced by comparing the sintering behavior of powder samples having equal geometry and initial porosity that are subjected to the same temperature and applied mechanical pressure but different current densities. In addition, several requirements should be met when choosing the experimental configurations and experimental set-ups. Firstly, the temperature should be measured inside the powder sample. Indeed, it is well known that the die temperature may significantly differ from that of the sample, the difference strongly depending on the experimental conditions. Secondly, the temperature and mechanical pressure gradients inside the powder sample should be minimized or controlled because their effect on the final product density can mask the intrinsic effect of the electric current.

Finally, the electric current flowing through a sample during SPS has to be evaluated. To the best of our knowledge,

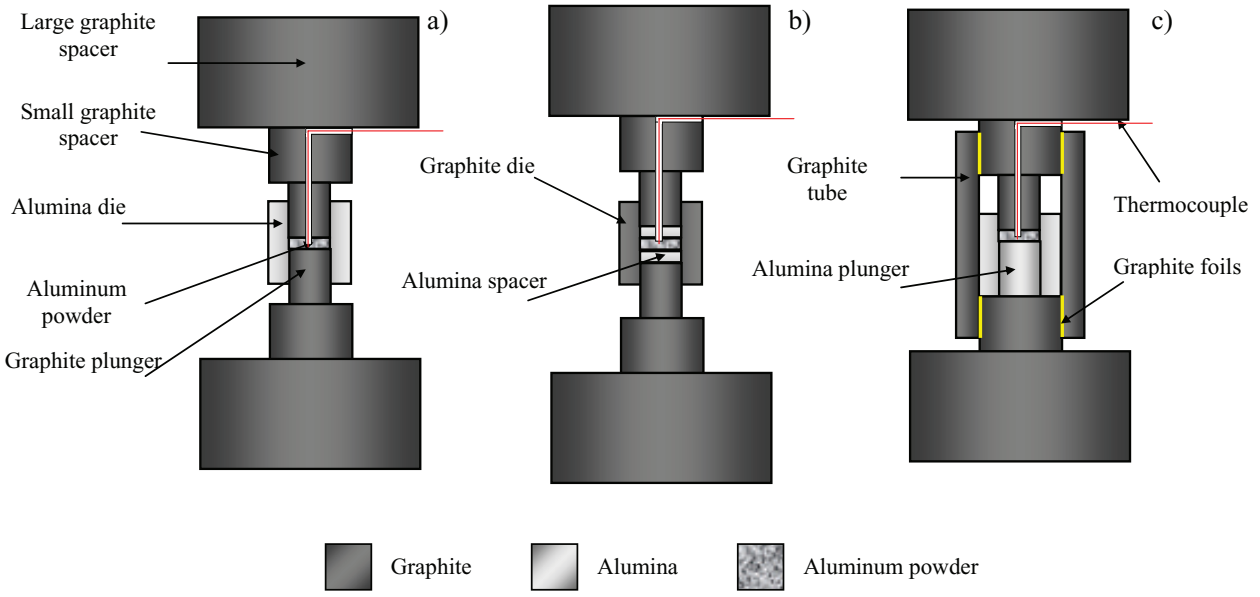

Figure 1. Schematic representation of ensemble configurations *A* (a), *B* (b), and *C* (c) adopted in the present investigation.

only one attempt to directly measure the current through a specimen during SPS has been reported to date [6]. However, several limitations and difficulties occurred during the measurement, casting doubt on the reliability of this technique. In addition, because the magnitude of the electric current passing through the sintering body as well as its spatial and temporal behavior are mutually affected by the sintering progress and the electrical properties of the sample, even the indirect evaluation of the current flowing through a sample is a difficult task.

Thus, a method to identify the intrinsic role of the electric current in SPS processes should be developed. To achieve this aim in the case of considering electrically conductive powders, a methodology is proposed in this work. Specifically, suitable ensemble configurations (geometry, size and material of the powder sample, die, plungers and spacers), in which the electric current is forced to flow only through the sample or the die, are first identified using a recently developed mathematical model [7]. The model is modified to account for heat transfer and generation, as well as the electric current flowing inside the powder sample.

To demonstrate this approach, we firstly analyzed the electrical and thermal behavior of specific experimental configurations. The potential intrinsic (non-Joule) effect of the electric current during the SPS of aluminum powder was then experimentally determined via sample shrinkage and final density using the ensemble configurations selected through the mathematical model.

2. Modeling section

In this work, we consider the three different ensemble configurations (heretofore named *A*, *B* and *C*) illustrated in figure 1. They are mathematically modeled as described below and analyzed from thermal and electrical viewpoints. Figure 1(a) shows configuration *A*, originally proposed by Weissler [8] in the framework of resistance sintering. Here, the powders contained in an alumina die allow the current to flow only through the sample. The plungers and spacers are made of graphite to complete the electric circuit. The basic idea of configuration *B* shown in figure 1(b) was proposed by Zadra *et al* [9] to investigate the SPS of aluminum powder. In this case, two alumina spacers are inserted between the graphite plungers and the powder. In this way, according to Zadra *et al* [9], the powder should be insulated from the conductive punches and no current should flow through it. The alternative configuration *C* shown in figure 1(c) is proposed in this work. Here, the powder is placed in an alumina die, and the upper and lower plungers are made of graphite and alumina, respectively. The electric circuit is completed by a graphite tube that surrounds the die and plungers and directly connects the small graphite spacers. The lower alumina plunger is expected to prevent the current from flowing through the sample and to force it to flow through the external graphite tube.

The configurations outlined above are simulated as inserted between the electrodes of an SPS 515S apparatus (Sumitomo Heavy Industries Ltd), which is described elsewhere [7]. The geometry, dimensions and materials of the elements of the arrangements shown in figure 1 are summarized in table 1, along with the size of the upper and lower stainless-steel electrodes (rams) provided with the SPS 515S apparatus.

Using the assumptions adopted in our previous work [7], the energy balance in cylindrical coordinates (r, z) related to the stainless-steel rams and the individual elements in figure 1

Table 1. Geometries, dimensions and materials of the elements constituting the simulated SPS ensembles *A*, *B* and *C*.

Element		Dimensions (cm)	Configuration *A*	Configuration *B*	Configuration *C*
Large graphite spacers		Height		4	
		Diameter		8	
Small graphite spacers		Height		2	
		Diameter		3	
Graphite plungers		Height		2	
		Diameter	1.5	1.5; 3	1.5
Alumina plunger		Height	–	–	2
		Diameter	–	–	1.5
Alumina spacers		Height	–	2; 4; 6	–
		Diameter	–	1.5; 3	–
Graphite die		Height	–	3	–
		Internal diameter	–	1.5; 3	–
		External diameter	–	3; 4.5; 6; 7.5	–
Alumina die		Height	3	–	3
		Internal diameter	1.5	–	1.5
		External diameter	3	–	3
Graphite tube		Height	–	–	7
		Internal diameter	–	–	3
		External diameter	–	–	4
Stainless-steel electrodes		Height (upper)		16.4	
		Height (lower)		26	
		Diameter		8	
Aluminum powder sample		Height	1	2; 4; 6	1
		Diameter	1.5	1.5; 3	1.5

is given as follows:

$$\rho_i C_{p,i} \frac{\partial T}{\partial t} = \frac{1}{r}\frac{\partial}{\partial r}\left(r k_i \frac{\partial T}{\partial r}\right) + \frac{\partial}{\partial z}\left(k_i \frac{\partial T}{\partial z}\right) + \frac{1}{\rho_{\mathrm{el},i}}\left[\left(\frac{\partial \varphi}{\partial r}\right)^2 + \left(\frac{\partial \varphi}{\partial z}\right)^2\right], \quad i = \begin{cases} \text{Stainless steel,} \\ \text{Graphite,} \\ \text{Alumina,} \\ \text{Powder.} \end{cases} \tag{1}$$

The thermal behavior of the powder sample, which was not considered in [7], is taken into account in this work using equation (1). The initial and boundary conditions pertaining to equation (1) are the same as those in [7], except for those related to the description of contact resistances. Indeed, only the horizontal contact resistances between electrodes and graphite spacers were considered in [7], whereas both the horizontal and vertical resistances between the ensemble components (figure 1) are taken into account in this work. In particular, the thermal contact resistances at each interface are modeled as shown in figure 2(a).

The steady-state conduction model

$$\frac{1}{r}\frac{\partial}{\partial r}\left(\frac{1}{\rho_{\mathrm{el},i}} r \frac{\partial \varphi}{\partial r}\right) + \frac{\partial}{\partial z}\left(\frac{1}{\rho_{\mathrm{el},i}} \frac{\partial \varphi}{\partial z}\right) = 0, \quad i = \begin{cases} \text{Stainless steel,} \\ \text{Graphite,} \\ \text{Alumina,} \\ \text{Powder.} \end{cases} \tag{2}$$

coupled with the boundary conditions given in [7] and figure 2(b) can be adopted to describe the electrical behavior of an SPS apparatus [7], including the features related to the powder sample and to the contact resistances between the ensemble components in figure 1.

An SPS apparatus typically includes a standard proportional-integral-derivative (PID) controller for

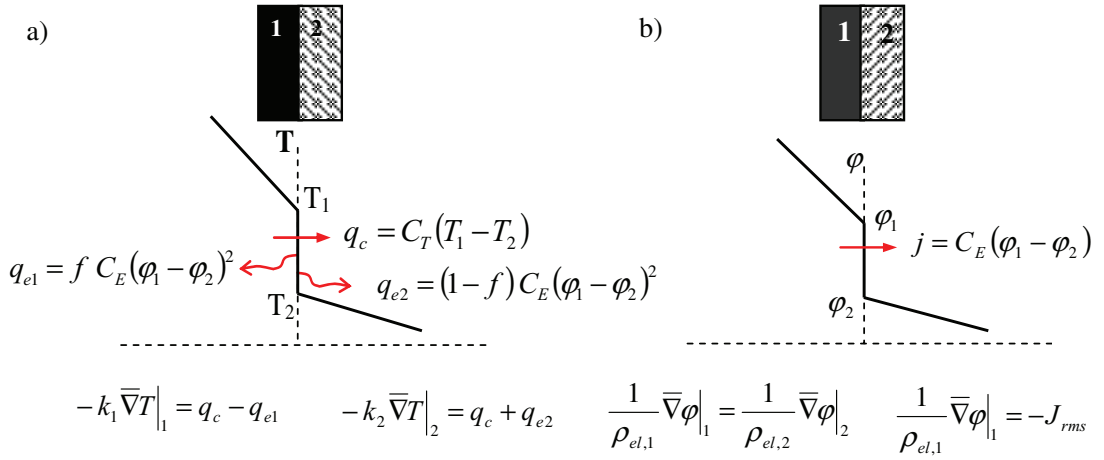

Figure 2. Boundary conditions at the contact interfaces: (a) thermal contact resistances and (b) electrical contact resistances.

Table 2. Model parameters.

Parameter	Value (unit)	Reference
K_P	1 A K^{-1}	This work
η_G	1	This work
η_{ss}	1	This work
$\eta_{Al_2O_3}$	1	This work
f	0.5	[7]
$\rho_{Al_2O_3}$	3986 kg m^{-3}	[12]
ρ_{Al}	2700 kg m^{-3}	[13]
τ_D	18 s	This work
τ_I	3 s	This work

temperature adjustment, which acts on the applied electric current. Therefore, to simulate temperature-controlled experimental runs, the mathematical model in [7] is improved by including the PID controller. Specifically, the root-mean-square (rms) electric current I_{rms}, which quantitatively determines the Joule effect during SPS, can be expressed as [10]

$$I_{rms}(t) = K_P\, e(t) + \frac{K_P}{\tau_I} \int_0^t e(t)\, dt + K_P \tau_D \frac{\partial e(t)}{\partial t}. \qquad (3)$$

Here, e represents the difference between the desired temperature (set-point) and the measured temperature. The meanings of the controller parameters K_P, τ_I, and τ_D in equation (3) are explained in the Nomenclature section. In this work, the measured variable is represented by the temperature of the powder sample determined as shown in figure 1.

The electric resistivity and thermal conductivity of the powder compact are evaluated using equations available in the literature [11]. Computational details of the numerical solution of the above differential, algebraic and integral equations can be found elsewhere [7]. Parameters used in the computations are reported in table 2 and figure 3 and in [7]. The only unknown model parameters are the thermal and electrical conductances, C_T and C_E, respectively, at the horizontal and vertical contacts between the different elements of the ensemble configurations (see figure 1 and the boundary conditions in figure 2). The values of these parameters are specified in the next section.

3. Modeling results and discussion

With the aim of developing a methodology to experimentally demonstrate, without potential misinterpretation of the corresponding results, the intrinsic effect of the pulsed electric current during the SPS of aluminum powders, we simulated the behavior of the arrangements depicted in figure 1. In particular, we analyzed the temperature and electric current distributions in the different elements of the ensembles. These distributions are strongly dependent on the thermophysical properties of the corresponding materials and on the electrical and thermal contacts resistances between the elements. While the thermophysical properties are readily available in the literature (see figure 3), the electrical and thermal contact resistances must be experimentally determined. This evaluation is time-consuming owing to the large number of contact interfaces (see figure 1). In addition, the contact resistances are strongly affected not only by the local temperature and pressure [7] but also by other factors that are difficult to control, such as the wear conditions of the surfaces; thus, the usefulness of their difficult experimental determination is limited. In this work, the contact resistances in model simulations were set as follows.

Our approach is based on the identification of suitable limiting values of the contact resistances and sample porosity. Thus, the model allows us to verify whether or not, for each considered ensemble, the applied current flows only through or only outside the sample and whether the axial and radial temperature gradients in the sample can be neglected.

Let us consider configuration *A* depicted in figure 1(a). Regarding the choice of the thermal contact resistances, it should be noted that higher temperatures are expected in the sintering sample. This is because of the smallest cross section and the porous structure of the sample. Therefore, the Joule effect is enhanced in the powder compact owing to its high electrical resistance. In addition, the larger distance of the sample from the cooling water system relative to the plungers slows down the heat removal. Consequently, heat transfer is expected to occur from the sample towards the die and the electrodes through the

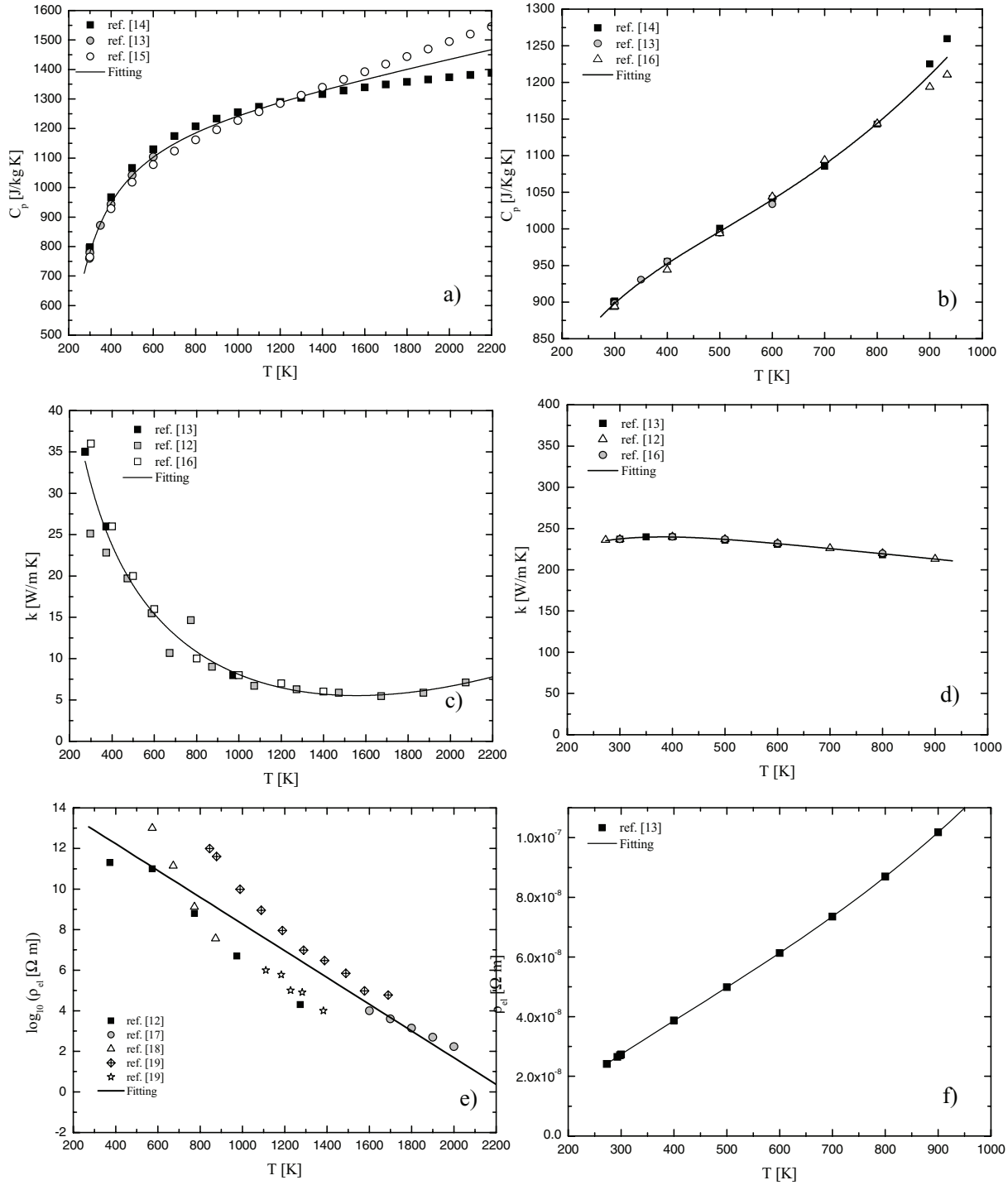

Figure 3. Thermophysical properties of alumina: (a) heat capacity, (c) thermal conductivity, (e) electrical resistivity and those of aluminum: (b) heat capacity, (d) thermal conductivity and (f) electrical resistivity.

plungers and spacers. Thus, to maximize the axial and radial temperature gradients inside the sample, all thermal contact resistances (both horizontal and vertical resistances) were neglected ($C_T \to \infty$) during the simulation runs. Indeed, if the contact resistances increase, then heat transfer from the hot sample to its surroundings is reduced (i.e. adiabatic conditions are approached), thus leveling out the temperature gradients. Accordingly, an analogous condition is also assumed for all the electrical contact resistances ($C_E \to \infty$). Specifically, we set $C_T = 1.0 \times 10^{12}\,\mathrm{W\,m^{-2}\,K^{-1}}$ and

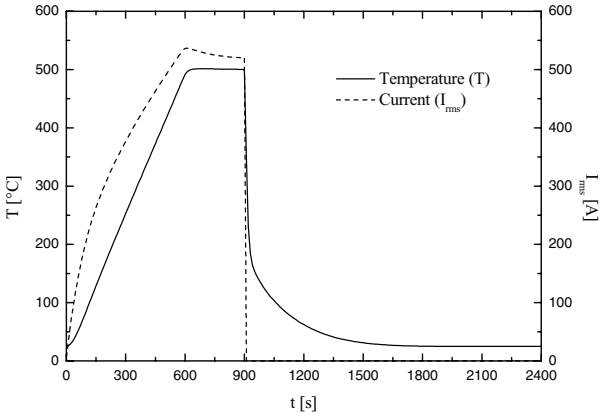

Figure 4. Simulated time profiles of the temperature at the sample center and the total current flowing in ensemble *A* during the SPS of aluminum powder.

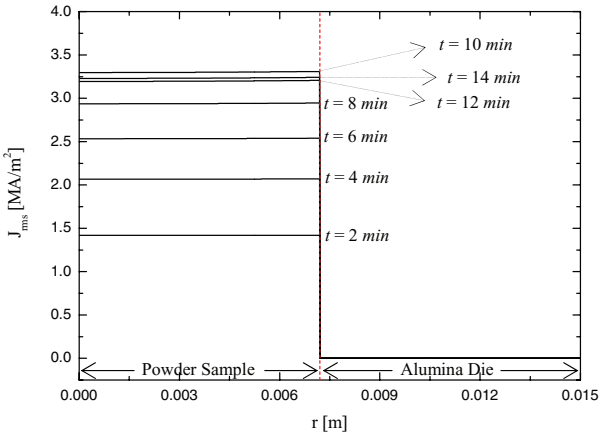

Figure 5. Simulated radial distribution of the rms electric current density inside ensemble *A* at the sample vertical center at different processing times during the SPS of aluminum powder.

$C_E = 1.0 \times 10^{12}\,\Omega^{-1}\,m^{-2}$. In addition, we consider a porous sample ($\varepsilon = 0.4$) that increases the electrical resistivity of the sample and emphasizes the thermal gradients. To this aim, we set the emissivities of each external surface to 1, thus increasing the heat losses to the surroundings even further.

It is apparent that by neglecting the vertical electrical contact resistances between the sample and the die and between the plungers and the die in the simulations, the electric current is allowed to flow through the die. Thus, if under such a limiting case, the model simulations predict that the applied current flows only through the sample and that the axial and radial temperature gradients inside the sample are negligible, then the same conclusions should hold for real and finite, albeit unknown, values of such parameters.

The thermal cycle adopted during the simulations consists of 10 min heating from room temperature ($T_0 = 25\,^\circ$C) to 500 °C followed by holding at this temperature for 5 min. Then, the electric current is interrupted and the system is allowed to naturally cool. The reliability of the simulated PID controller is shown in figure 4, which illustrates the simulated time profile of the temperature at the center of an aluminum powder sample. It can be seen that the system temperature follows the desired set-point temperature. Figure 4 also shows the simulated total current flowing inside ensemble *A*.

Figure 5 shows the simulated radial distribution of the rms electric current density at the vertical center of the sample (ensemble *A*). As expected, the current is confined in the aluminum sample owing to the very high electrical resistivity of the alumina die. Therefore, because these results are related to the limiting-case simulation described above, the electric current only flows through the processed powders, independent of the actual values of vertical electrical contact resistances.

Figure 6 shows the calculated temperature differences established inside the sample during the SPS process under the same limiting-case conditions. These differences are quite small, less than 3.5 °C, owing to the relatively high thermal conductivity of aluminum and the small sample size. Consequently, these temperature differences are the largest

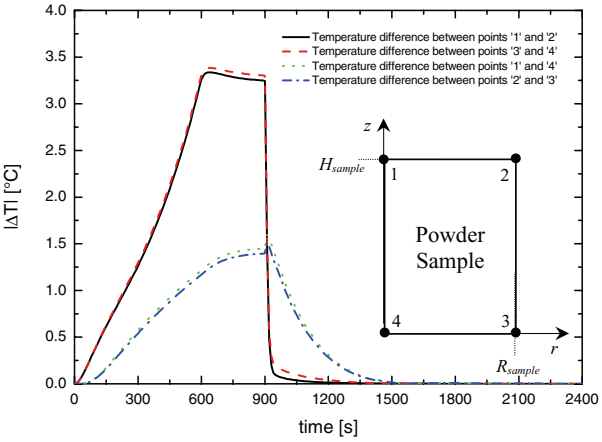

Figure 6. Simulated time profiles of temperature differences (absolute values) between specific sample locations during the SPS of aluminum powder when considering ensemble *A*.

achievable under the imposed temperature profile shown in figure 4. If the horizontal and vertical thermal contact resistances had not been neglected, then the calculated heat fluxes from the sample towards the plungers, spacers and electrodes as well as towards the die would have decreased, thus reducing the axial and radial temperature gradients inside the sample, respectively. The results of the numerical simulations (not shown here for brevity) confirm these conclusions. Furthermore, powder consolidation during the process should reduce the sample porosity, thus increasing the thermal conductivity of the sample. Although this phenomenon is not modeled in this work for the sake of simplicity, even smaller temperature gradients are expected during actual SPS under the adopted experimental conditions. Thus, from this simulation of ensemble *A*, the temperature measured inside the sample can be safely used to represent that of the whole sample and the applied electric current may be considered as flowing exclusively through the sample.

Zadra *et al* [9] adopted a configuration similar to that shown in figure 1(b) to spark plasma sinter aluminum powder.

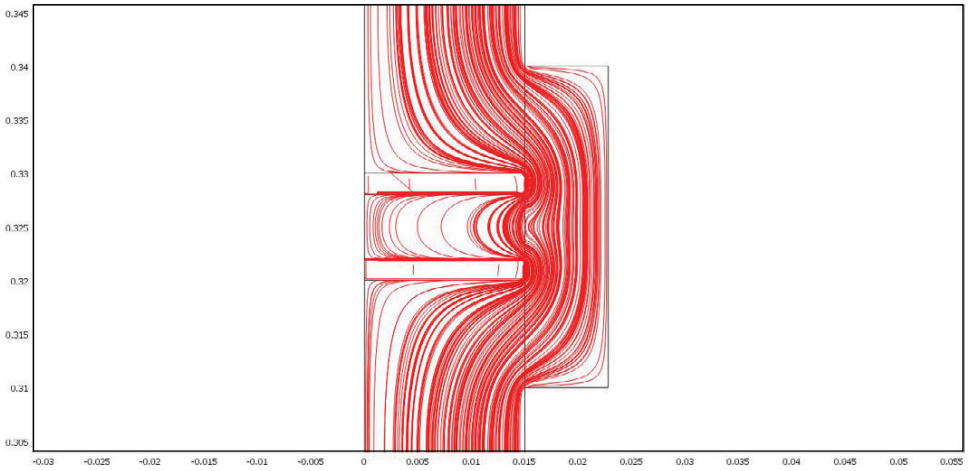

Figure 7. Simulated electric current distribution within the ensemble of Zadra *et al* during the SPS of aluminum powder at processing time $t = 5$ min.

It was claimed that two alumina spacers (2 mm thick) placed between the plungers and the powder sample (30 mm diameter and 6 mm height) electrically insulated the sample from the conductive graphite plungers. However, this assumption was neither verified experimentally nor supported by model simulations. Therefore, we also carried out simulations of Zadra *et al* configuration. It should be noted that whereas the experimental runs were conducted using the same SPS apparatus considered this work, Zadra *et al* did not use small spacers [9]. Consequently, in our simulation, we excluded the small spacers from the ensemble. In addition, we set the external die diameter not reported therein to 45 mm, whereas the other dimensions are summarized in table 1.

Following the adopted approach, we neglected all the electrical contact resistances and set the relative density of the sample to 1, i.e. the ratio of the sample to bulk densities. In this way, the most favorable conditions for the flow of the current inside the powder sample are considered. Accordingly, all the thermal contact resistances were also neglected in this simulation. Specifically, we set $C_T = 1.0 \times 10^{12}$ W m^{-2} K^{-1} and $C_E = 1.0 \times 10^{12}$ Ω^{-1} m^{-2} and used the same temperature cycle as that for ensemble *A*, which is similar to that used in the experiment by Zadra *et al* [9].

The streamline plot of figure 7 shows the simulated electric current distribution within the arrangement of Zadra *et al* at $t = 5$ min. The electric current bends and flows also inside the aluminum sample. This is probably due to the very high electrical conductivity of aluminum, which is higher than that of graphite. This makes the path through the sample less resistive for the current portion flowing close to the boundary between sample and die. To clarify these results, it is worth defining the cumulative fraction of the total current flowing through a section of radius r perpendicular to the z-axis as

$$\Phi(r, t) = \frac{4\pi}{I_{\mathrm{rms}}(t)} \int_0^r J_{\mathrm{rms}}(r, t) r \, \mathrm{d}r. \qquad (4)$$

The radial distribution of this variable and that of the rms electric current density at $t = 5$ min are shown in figure 8.

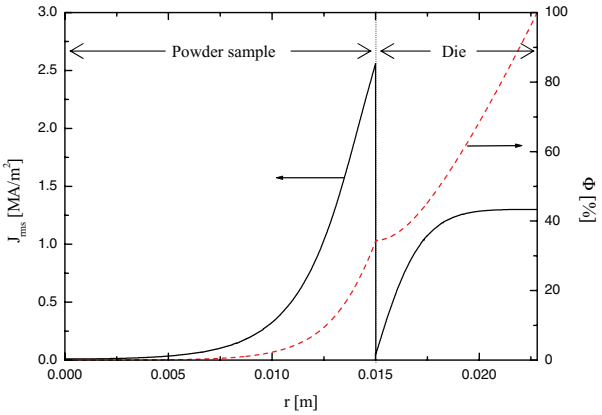

Figure 8. Simulated radial distribution of the rms electric current density within the ensemble of Zadra *et al* at the vertical center of the sample at $t = 5$ min during the SPS of aluminum powder.

The current density inside the sample is relatively high, i.e. about 34% of the total current flowing in the system (at the vertical center of the sample) is discharged through the powder compact.

This analysis performed using our model, whose reliability have been previously demonstrated [7], clearly demonstrates that the ensemble proposed by Zadra *et al* [9] does not guarantee that the electric current flows exclusively outside the sample. Certainly, higher sample porosity and electrical contact resistances between the sample and the die may decrease the fraction of current flowing through the specimen. However, during sintering, the specimen porosity decreases and the electric contact resistances may vary depending on temperature and pressure distributions. Therefore, the configuration of Zadra *et al* cannot be confidently chosen *a priori* to perform SPS experiments in which the electric current is needed to flow only through the die.

We performed additional simulations to examine whether the fraction of the electric current passing through the sample

Table 3. Effect of ensemble dimensions on the fraction of current flowing through the sample.

Sample thickness (mm)	Alumina spacer thickness (mm)	External die diameter (mm)	Total current (A)	Current flowing through the sample (%)[a]
2	2	75	1786	7.63
2	4	75	1674	6.24
2	6	75	1572	5.57
4	2	75	1732	14.2
6	2	45	1549	34.0
6	4	60	1645	22.0
6	6	75	1679	20.0

[a]Calculated using equation (4) with the integral upper limit equal to the sample radius.

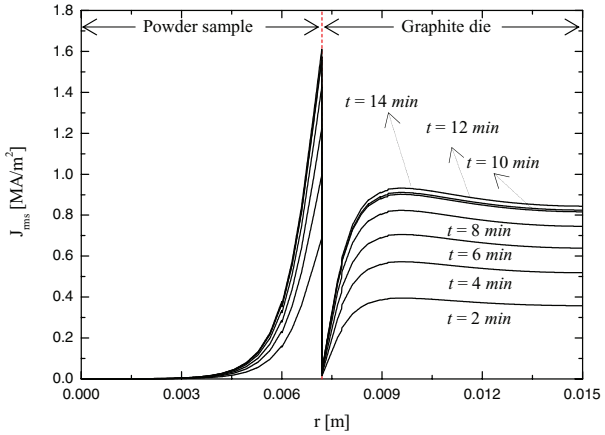

Figure 9. Simulated radial distribution of the rms electric current density inside ensemble *B* at the sample vertical center at different processing times during the SPS of aluminum powder.

varies with the dimensions of the sample, the alumina spacers and the die, and the results are summarized in table 3. The total current flowing through the specimen decreases with decreasing sample height, with increasing thickness of the spacers and with increasing diameter of the external die. However, these results demonstrate that it is difficult to identify the dimensions of Zadra *et al* ensemble in which the current flow through the sample can be excluded.

The numerical results presented in figure 9 show that, even for configuration *B* with identical geometry and dimensions (except for the presence of alumina spacers) to those of arrangement *A*, the current density through the sample is still significant. Thus, also configuration *B* is not suitable for investigating the intrinsic effect of the electric current during SPS. In particular, the recent study by Misawa *et al* [6], which compared results obtained using arrangements *A* (equipped with a graphite die instead of an alumina die) and *B*, might be inconclusive.

Let us now consider configuration *C* (figure 1(c)) in which the electric current may potentially flow through the following two paths. It may flow from the upper electrode to the upper small spacer, then through the graphite tube toward the lower small spacer, and then to the lower electrode (path α). Alternatively, the current may flow from the upper small spacer through the upper graphite plunger and then through the sample, the alumina plunger and the alumina die (path β). The redistribution of the current between these two paths strongly depends on the involved bulk and contact electric resistances. High vertical electrical contact resistances between the graphite tube and the touching elements, while neglecting all the remaining electrical resistances, undoubtedly represents the most favorable condition for the flow of current along path β. However, the highest electrical resistance along path β is given by that of the alumina plunger and alumina die ensemble (about $2.8 \times 10^{12}\,\Omega$). This means that by applying the maximum voltage (10 V) attainable in the simulated SPS 515S apparatus, the current flowing through path β should be approximately 3.5×10^{-12} A. This is a very low value compared with a typical total current in the SPS process (10^2–10^3 A). Therefore, it can be safely assumed that the electric current is forced to flow along path α regardless of the electrical contact resistances. This assumption has also been verified experimentally by inserting ensemble *C* without the graphite tube between the electrodes of the SPS apparatus. A voltage of about 10 V was measured but no current could be detected under the above simulated experimental conditions. Similar theoretical and experimental results were obtained by Carney and Mah when attempting to restrict the electric current to flowing through alumina samples [20]. Thus, we may conclude that the electrical contact resistances in ensemble *C* may affect the total current flowing through the system, but its distribution among the different elements should not be affected.

Regarding the temperature distribution within configuration *C*, the thermal contact resistances should be set so as to enhance the temperature gradients inside the sample. As the electric current is assumed to flow only through the graphite tube, the sample is heated by conduction from the contacting elements. Model simulations, not reported here for brevity, show that the maximum temperature gradient inside the sample increases if the vertical and horizontal thermal contact resistances increase and decrease, respectively. Decreasing the horizontal thermal contact resistances enhances the heat flux from the plungers and small spacers towards the sample, thus increasing the axial temperature gradients within the sample. An increase in the vertical thermal contact resistances corresponds to a decrease in the heat flux from the die towards the sample, thus maximizing the radial temperature gradients. Therefore, in model simulations the vertical thermal contact resistances are maximized, and all others (horizontal and vertical electric resistances and horizontal thermal resistances) are neglected. Specifically, we set the horizontal thermal conductances to $1.0 \times 10^{12}\,\mathrm{W\,m^{-2}\,K^{-1}}$, the vertical thermal conductance to zero and all electrical conductances to $1.0 \times 10^{12}\,\Omega^{-1}\,\mathrm{m^{-2}}$. In addition, to further increase temperature gradients, we consider a relatively high porous sample ($\varepsilon = 0.4$) that lowers the thermal conductivity. We also assumed an emissivity of 1 for each external surface to maximize the heat losses.

Figure 10 shows the simulated time dependence of temperature at the center of the aluminum sample and that of the total rms current flowing through the system. The set-point

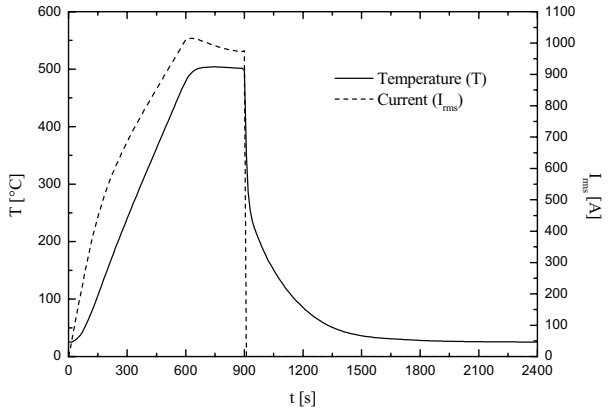

Figure 10. Simulated time profiles of the temperature at the sample center and the total current flowing in ensemble *C* during the SPS of aluminum powder.

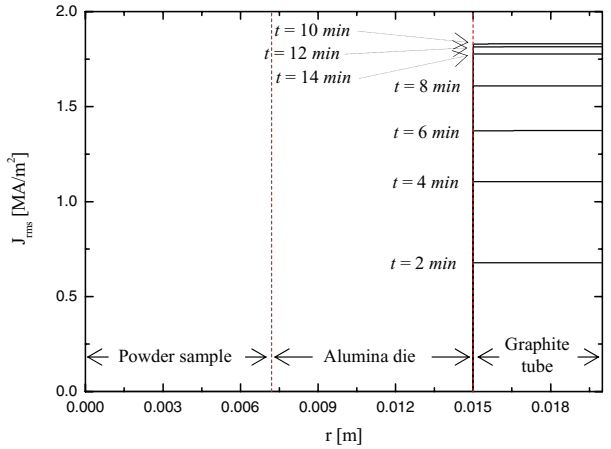

Figure 11. Simulated radial distribution of the rms electric current density inside ensemble *C* at the sample vertical center at different processing times during the SPS of aluminum powder.

temperature cycle is identical to that adopted for ensembles *A* and *B*. The reliability of the simulated PID controller is clearly demonstrated also in this case.

Figure 11 shows the calculated temporal evolution of the radial distribution of the rms electric current density inside the ensemble at the vertical center of the powder sample. It confirms that the current is confined to the graphite tube at any time. Figure 12 shows the calculated temperature differences arising in the sample during the SPS process. The differences are relatively small (<16 °C) owing to the high thermal conductivity and the small size of the aluminum sample. Because of our setting of the contact resistances, the calculated temperature differences are the highest achievable under the chosen operative conditions. Furthermore, powder consolidation during SPS should reduce sample porosity and increase its thermal conductivity, and thus further reduce the temperature gradients. Therefore, if configuration *C* is adopted to investigate the intrinsic effect of the electric current, the temperature measured inside the sample should represent that of the whole sample, and the current flowing through it may be neglected.

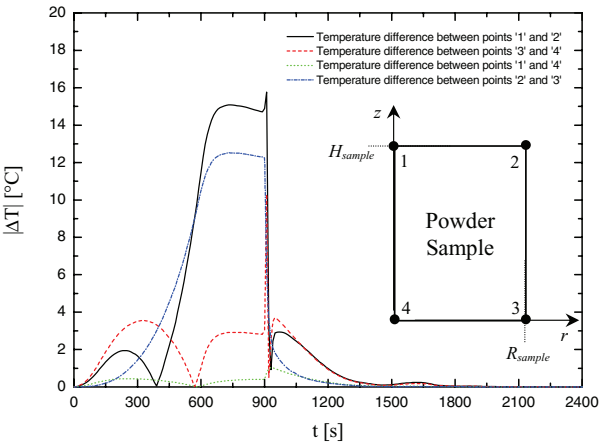

Figure 12. Simulated time profiles of temperature differences (absolute values) between specific sample locations during the SPS of aluminum powder when considering ensemble *C*.

On the basis of the above analysis, we chose ensembles *A* and *C* to experimentally investigate the intrinsic effect of the electric current during the SPS of aluminum powder. Accordingly, experimental runs were performed as illustrated in the next section.

4. Experimental section

An SPS apparatus (model 515S, Sumitomo Coal Mining Co. Ltd, Japan) was used to consolidate aluminum powder (Aldrich, cat.no 21,475-2, −200 mesh, 99% purity) by adopting configurations *A* and *C*. All graphite elements were made of AT101 graphite (Atal s.r.l., Italy) and the alumina die and plunger were supplied by francoCorradi (Italy). The die was filled with 1.9 g of powder. To ensure a closed electric circuit in ensemble *C*, a 99.8% pure graphite foil (0.13 mm thick, Alfa Aesar, Germany) was inserted between the internal surface of the tube and the lateral surfaces of the small spacers. The ensembles were then placed between the upper and lower electrodes of the sintering chamber of the SPS apparatus and the system was evacuated to 10 Pa.

The set-point temperature cycle was set to be the same as that simulated in the previous section. The adopted electric current pulse pattern consists of 12 on-pulses and 2 off-pulses with a total duration of 46.2 ms and a pulse duration of 3.3 ms. The applied mechanical pressure (*P*) was 20 MPa for all experiments.

The temperature during sintering was measured using a C-type thermocouple (model No. W5W26-005, Omega Engineering Inc., UK) inserted inside a small hole axially drilled in the center of the upper graphite small spacer and plunger, as shown in figure 1. The temperature, rms current and voltage, mechanical load, and the vertical displacement of the lower electrode were measured in real time and recorded using an acquisition system described elsewhere [7]. The vertical displacement of the lower electrode may be related to the degree of powder densification. The thermal expansion of the sample and of all parts comprising each ensemble also

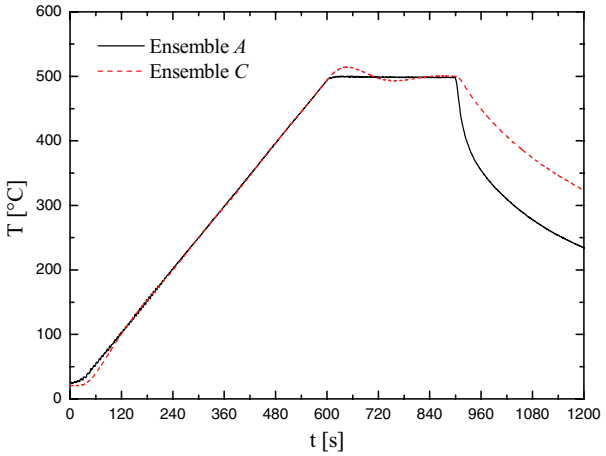

Figure 13. Experimental time profiles of sample temperature measured during the SPS of aluminum powder.

contributes to the vertical displacement. This contribution was evaluated by performing a 'blank test', which consisted of applying the same SPS conditions (current, mechanical load, time, etc) to the ensembles without a sample inside. The sample shrinkage (δ) was obtained by subtracting the resulting displacement from that recorded with powder. However, the thermal expansion of the sample itself could not be accounted for in this way.

The relative density of the sintered samples was determined using the Archimedes method with distilled water as wetting liquid. Each experiment was repeated four times.

5. Experimental results and discussion

Figure 13 shows the time profile of temperature measured during the SPS experiments for the two selected configurations *A* and *C*. An overshoot with a maximum at 516 °C is seen for arrangement *C*. However, the temperature difference between ensembles *A* and *C* is always less than 18 °C (the average difference is 4 °C). Therefore, excluding the cooling stage, samples sintered using these two configurations practically experienced the same temperature cycle during the SPS runs.

Figure 14(a) shows the measured rms electric current applied to configurations *A* and *C*. The current increases during the heating stage (see figure 13) up to about 400 and 650 A for ensemble *A* and *C*, respectively. Once the holding temperature is reached, the temperature controller reduces the applied current. The oscillatory behavior of the applied current for configuration *A* (magnified in the inset of figure 14(a)) is discussed below. Figure 14(b) shows the corresponding time profile of the voltage, which also exhibits oscillations.

Figure 15 shows time profiles of sample shrinkage (δ) for both configurations. As mentioned above, the thermal expansion of the sample can alter absolute value of specimen shrinkage. However, because the sample weight and dimensions are the same, the temperature cycle experienced by the sample are similar (see figure 13), and the temperature

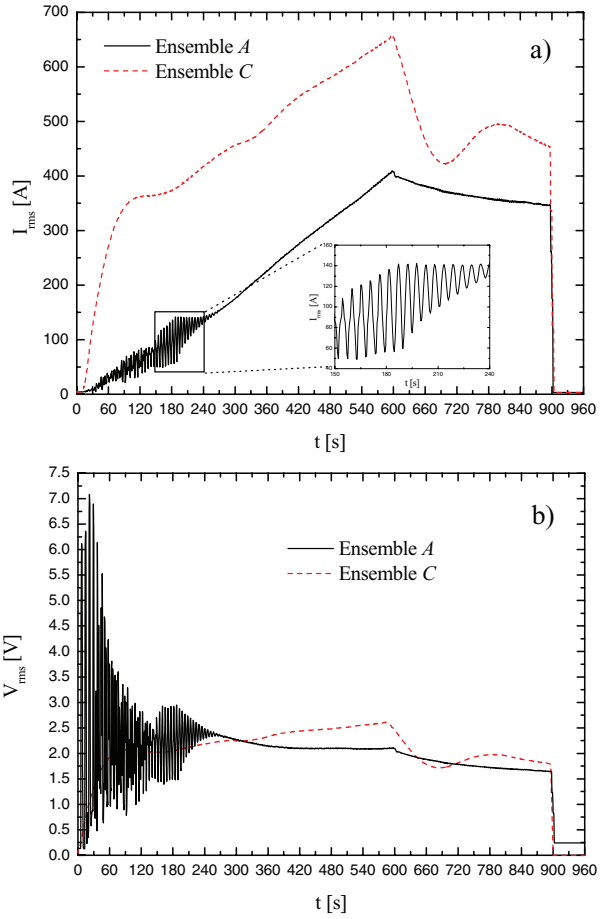

Figure 14. Experimental time profiles of (a) rms electric current applied during the SPS of aluminum powder and (b) the corresponding rms voltage.

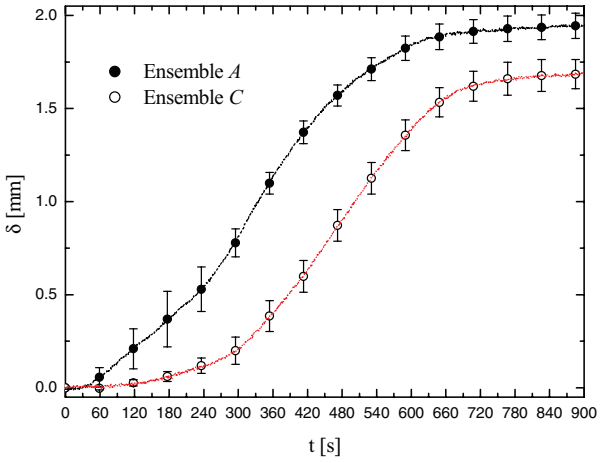

Figure 15. Experimental time profiles of powder sample shrinkage measured during the SPS of aluminum powder.

gradients within the sample are limited (see figures 6 and 12), it is reasonable to assume that the thermal expansion did not significantly affect the difference between the two shrinkage curves.

The sample shrinkage, and thus the sample density, is higher for ensemble *A*. Specifically, the final sample shrinkages are 1.94 mm and 1.69 mm for configurations *A* and *C*, respectively. The density for configuration *A* is $2481.75^{+0.32\%}_{-0.31\%}$ kg m^{-3}, which is equivalent to a relative density of 91.92%. The corresponding values for arrangement *C* are $2361.01^{+0.60\%}_{-0.87\%}$ kg m^{-3} and 87.45%. The difference between the densities for configurations *A* and *C* (about 5%) is larger than the experimental error (about 1%).

Before discussing these results, we would like to comment on the experimental setup (see figure 1). First, it should be stressed that the temperature is measured at the center of the top surface of the sample for both ensembles *A* and *C*. In addition, the temperature differences inside the aluminum powder samples calculated using our model and the above-described approach, do not exceed about 4 °C and 16 °C for arrangements *A* and *C*, respectively, under the experimental conditions used in this work. Therefore, the whole aluminum powder sample should have been at the same temperature in both configurations *A* and *C*. Thus, the measured differences in shrinkage and density cannot be ascribed to dissimilar temperatures experienced by the two samples.

Regarding the mechanical load, the same nominal pressure was applied during SPS runs for both configurations. However, we should consider the effect of friction between the small graphite spacers and the graphite tube in ensemble *C* (see figure 1). Indeed, the force acting along the radial direction due to the thermal expansion of the small graphite spacers and/or graphite tube may cause an axial friction force counteracting the applied mechanical pressure. Therefore, the actual pressure acting on the sample may be lower than the nominal pressure for ensemble *C*. However, this effect should be negligible owing to the low friction coefficient and Young's modulus of the flexible graphite foils inserted between the graphite tube and small spacers.

Friction between the powder sample and alumina die may potentially generate pressure gradients inside the sample, thus inducing density gradients within the sintered compact. However, this effect should be similar on both configurations since samples are subjected to the same temperature and pressure fields. Therefore, the density differences between the samples obtained using ensembles *A* and *C* should not be related to pressure effects.

On the other hand, these two arrangements differ only in the electric current distribution inside the system. In particular, the current flows only through the sample in configuration *A*, and only through the graphite tube in configuration *C*. Thus, the specimen in configuration *A* is heated by the Joule effect due to the current flowing through it, whereas the temperature of the sample in configuration *C* is increased through thermal conduction from the graphite tube and small spacers. Hence, the difference in shrinkage behavior shown in figure 15 as well as the higher final density of sample *A* may be ascribed to the intrinsic effect of the electric current on the sintering process.

As mentioned in the introduction, the aim of this work was to develop a methodology to highlight the potential non-Joule effect of the electric current in the SPS of electrically conductive powder. At this stage, an intrinsic effect of the electric current on powder densification was experimentally observed for aluminum powder. However, we neither want to generalize this result for other powders nor claim that this is the only effect on SPS of aluminum powder. Moreover, it is not our intention to discuss the magnitude of such an effect on the density of aluminum samples.

Further investigations of this effect are necessary. The relative importance of the intrinsic role of the electric current during SPS may depend on the experimental conditions, such as the heating rate, temperature, and mechanical pressure, as well as electrical conductivity and particle size of the powder. The analysis of the few previously reported experimental results on this matter is not conclusive. In fact, an intrinsic effect of the application of a pulsed electric current have been experimentally observed only on the solid-state diffusion during steel plates boriding [21] and on reactivity during diffusion couples experiments [22–24]. On the other hand, by imposing the same temperature and mechanical pressure, similar densities and microstructures were observed in electrically conductive ceramic samples heated by either restricting the current to flow only through the powder or with current allowed to pass through both the graphite die and the powder [20]. Further experimental investigations conducted following the proposed approach may shed light on the behavior of aluminum powder under different operating conditions or of other electrically conductive powder.

Regarding a possible explanation of our results, numerous mechanisms and effects have been proposed in the literature in order to elucidate the fundamentals of the SPS process. Among these, the local Joule heating at the contacts between individual particles [4, 25, 26] may represent a realistic explanation of the experimental results shown in this work. The small contact areas and the typical presence of oxide layers covering the aluminum particles may significantly increase the electrical resistance of the compact. Thus, the relatively high current density at these contact points can raise at the initial stage of the SPS the local (i.e. at the particle contacts) temperature to above the one measured in the bulk of the sample using thermocouples. Local overheating can cause melting and/or evaporation, leading to an increase in the plastic deformation and mass transport. Eventually, an increase in mass transport can promote neck formation between particles, thereby enhancing the sintering rate.

This mechanism has been reported to be particularly active in the early stage of the SPS process [4], i.e. when the sample porosity is still high. The shrinkage time profiles in figure 15 may support this hypothesis. A larger difference in the sintering rate between the two experimental profiles is observed during the first part of the heating (up to about 5 min). It is plausible to assume that as the sample density increases, the contact area between the particles increases and the difference between the bulk and the local temperatures vanishes. Consequently, the sintering rates for the samples in

configurations *A* and *C* tend to become similar from about 5 min until the end of the process (see figure 15).

The high electrical resistance of the porous aluminum sample at the beginning of the SPS process may also explain the oscillatory behavior of the applied electric current shown in figure 14. A local temperature rise should increase the electrical resistivity of aluminum (see figure 3(f)). This increase causes the PID controller to reduce the electric current to follow the desired temperature cycle. The reduction of the current density decreases the local temperature and thus the electrical resistivity of the sample. Thus, oscillatory behavior may arise until the sample porosity is reduced.

6. Summary

We have carried out a study of the intrinsic effect of the pulsed electric current during the SPS of electrically conductive powders. To avoid the misinterpretation of experimental results, three configurations (with different geometries, sizes and materials of the die, plungers and spacers) were analyzed from electrical and thermal viewpoints. A suitable mathematical model was adopted, which describes the heat transfer and generation, and flow of the electric current during the SPS process inside the ensemble individual elements (electrodes, spacers, plungers, die, powder sample, etc). In this way, suitable ensembles were selected as capable of experimentally highlighting the potential intrinsic (non-Joule) effects of the electric current. Specifically, the geometry, sizes, and materials of two different configurations were identified as being suitable for analyzing the SPS of aluminum powder. In the first ensemble, the electric current is forced to flow inside the sample by containing it in an alumina die. In this case, compact heating is achieved through the Joule effect in the aluminum powders. In the second ensemble, which had a more complex arrangement, the current is forced to flow outside to the powder and, the sample is heated through thermal conduction only. The temperature gradients within the samples were minimized in both configurations.

On the basis of the modeling results, an experimental investigation of the intrinsic effect of the electric current during the SPS of aluminum powder was carried out using the two designed ensembles. Under the experimental conditions taken into account, it was found that the final density of samples obtained when the electric current flows through the sintering powder is about 5% higher than that when the samples are processed using the same temperature cycle and mechanical pressure but when the electric current flows only outside the sample.

Acknowledgment

Innovative Materials s.r.l. (Italy) is gratefully acknowledged for granting the use of the SPS apparatus.

References

[1] Orrù R, Licheri R, Locci A M, Cincotti A and Cao G 2009 *Mater. Sci. Eng.* R **63** 127
[2] Grasso S, Sakka Y and Maizza G 2009 *Sci. Technol. Adv. Mater.* **10** 053001
[3] Munir Z A, Anselmi-Tamburini U and Ohyanagi M 2006 *J. Mater. Sci.* **41** 763
[4] Mamedov V 2002 *Powder Metall.* **45** 322
[5] Dobedoe R S, West G D and Lewis M H 2003 *Bull. Eur. Ceram. Soc.* **1** 19
[6] Misawa T, Shikatani N, Kawakami Y, Enjoji T, Ohtsu Y and Fujita H 2009 *J. Mater. Sci.* **44** 1641
[7] Cincotti A, Locci A M, Orrù R and Cao G 2007 *AIChE J.* **53** 703
[8] Weissler GA 1981 *Int. J. Powder Metall. Powder Technol.* **17** 107
[9] Zadra M, Casari F, Girardini L and Molinari A 2007 *Powder Metall.* **50** 40
[10] Stephanopoulos G 1984 *Chemical Process Control: An Introduction to Theory and Practice* (Englewood Cliffs, NJ: Prentice-Hall)
[11] Montes J M, Cuevas F G and Cintas J 2007 *Metall. Mater. Trans.* B **38** 957
[12] CRC 2001 *Materials Science and Engineering Handbook* 3rd edn (Boca Raton, FL: CRC)
[13] CRC 2000 *Handbook of Chemistry and Physics* 80th edn (Boca Raton, FL: CRC)
[14] Barin I 1993 *Thermochemical Data of Pure Substances* (Weinheim: VCH)
[15] Kubaschewski O and Evans E L 1951 *Metallurgical Thermochemistry* (London: Butterworth-Springer Ltd)
[16] Perry R H and Green D 1984 *Perry's Chemical Engineers' Handbook* 6th edn (New York: McGraw-Hill)
[17] Pappis J and Kingery W D 1961 *J. Am. Ceram. Soc.* **44** 459
[18] Moulson A J and Herbert J M 1990 *Electroceramics: Materials, Properties, Applications* (London: Chapman and Hall)
[19] IIT Research Institute 1961 *Handbook of Thermophysical Properties of Solid Materials* (London: Macmillan)
[20] Carney C M and Mah T I 2008 *J. Am. Ceram. Soc.* **91** 3448
[21] Yu L G, Khor K A and Sundararajan G 2002 *Surf. Coat. Technol.* **157** 226
[22] Anselmi-Tamburini U, Garay J E, Groza J R and Munir Z A 2005 *Mater. Sci. Eng.* A **407** 24
[23] Kondo T, Kuramoto T, Kodera Y, Ohyanagi M and Munir Z A 2008 *J. Ceram. Soc. Japan* **116** 1187
[24] Kondo T, Yasuhara M, Kuramoto T, Kodera Y, Ohyanagi M and Munir Z A 2008 *J. Mater. Sci.* **43** 6400
[25] Omori M, Okubo A, Gilhwan K and Hirai T 1997 *J. Mater. Synth. Process.* **5** 279
[26] Moon K, Kim S C and Lee K S 2002 *Intermetallics* **10** 185